ADVANCED FUNCTIONAL MATERIALS
www.afm-journal.de

Materials Views
www.MaterialsViews.com

Omniphobic "R^F Paper" Produced by Silanization of Paper with Fluoroalkyltrichlorosilanes

*Ana C. Glavan, Ramses V. Martinez, Anand Bala Subramaniam, Hyo Jae Yoon, Rui M. D. Nunes, Heiko Lange, Martin M. Thuo, and George M. Whitesides**

The fabrication and properties of "fluoroalkylated paper" ("R^F paper") by vapor-phase silanization of paper with fluoroalkyl trichlorosilanes is reported. R^F paper is both hydrophobic and oleophobic: it repels water ($\theta_{app}{}^{H}2^{O}$>140°), organic liquids with surface tensions as low as 28 mN m^{-1}, aqueous solutions containing ionic and non-ionic surfactants, and complex liquids such as blood (which contains salts, surfactants, and biological material such as cells, proteins, and lipids). The propensity of the paper to resist wetting by liquids with a wide range of surface tensions correlates with the length and degree of fluorination of the organosilane (with a few exceptions in the case of methyl trichlorosilane-treated paper), and with the roughness of the paper. R^F paper maintains the high permeability to gases and mechanical flexibility of the untreated paper, and can be folded into functional shapes (e.g., microtiter plates and liquid-filled gas sensors). When impregnated with a perfluorinated oil, R^F paper forms a "slippery" surface (paper slippery liquid-infused porous surface, or "paper SLIPS") capable of repelling liquids with surface tensions as low as 15 mN m^{-1}. The foldability of the paper SLIPS allows the fabrication of channels and flow switches to guide the transport of liquid droplets.

1. Introduction

The design of devices that handle liquids, or control the transport of gases, would benefit from new materials, and from repurposing currently available materials to have new properties and functions. To channel or restrict the flow of liquids requires non-permeable materials; to transport gases requires porous media. Porous, water-repellent materials based on expanded polytetrafluoroethylene (ePTFE, Gore-Tex, Nafion, Teflon) and other polymers have been useful in a wide range of applications, from high performance fabrics and membrane filters to fuel cells,[1] surgical implants,[2–5] and lung-assist devices.[6,7] The relatively high cost (from ~USD$1500 m^{-2} for Nafion to ~$29 m^{-2} for Gore-Tex) of these materials has, however, limited their utilization for applications requiring a low-cost or single-use format.

Paper is a useful substrate in applications that require low cost, flexibility, disposability, porosity, and adaptability to large-scale manufacturing.[8–11] In recent years, it has become increasingly popular as a material for the construction of "high-tech" devices in consumer electronics,[12–14] chemical and physical microelectromechanical systems (MEMS) sensors,[8,15–17] user interfaces,[18] electronic displays,[19] cell-based assays[20] and microfluidic devices.[10,21] The tendency of paper to absorb solvents (including water), however, limits its adoption as a substrate in liquid-handling applications in which wicking is not desirable, or in which moisture and humidity can cause deleterious effects (especially changes in mechanical and electrical properties). For such applications, paper must be made resistant to wetting by liquids, and to adsorption of liquids (especially water) from the atmosphere.

This work describes a rapid, simple method for altering the surface chemistry of paper by treatment with organosilanes in the gas phase. Reaction of paper with alkyl trichlorosilanes rendered paper resistant to wetting by high surface tension liquids such as water, while preserving the flexibility and low resistance to the passage of gas of the untreated paper. We compared the wetting behaviors of three papers of different surface topographies (determined through root mean square roughness ($R_{R.M.S.}$) measurements)—each functionalized with organosilanes of different alkyl chain lengths, and different levels of fluorination—to characterize systematically the contributions surface chemistry and topography to the wetting properties of the modified paper.

Treatment of all three papers with fluorinated alkyl trichlorosilanes made them resistant to wetting by both water and non-polar liquids such as n-hexadecane. The "fluoroalkylated paper," or "R^F paper" is thus omniphobic (i.e., both hydrophobic and oleophobic). R^F paper repelled liquids spanning a broader range of

A. C. Glavan, Dr. R. V. Martinez,[+]
Dr. A. B. Subramaniam,[+] Dr. H. J. Yoon,
Dr. R. M. D. Nunes, Dr. H. Lange, Dr. M. M. Thuo,
Prof. G. M. Whitesides
Department of Chemistry and Chemical Biology
Harvard University
12 Oxford Street, Cambridge, MA, 02138, USA
E-mail: gwhitesides@gmwgroup.harvard.edu
Dr. R. V. Martinez
Madrid Institute for Advanced Studies
IMDEA Nanoscience
Calle Faraday 9, Ciudad Universitaria de Cantoblanco, 28049, Madrid, Spain
Prof. G. M. Whitesides
Wyss Institute for Biologically Inspired Engineering
Harvard University
60 Oxford Street, Cambridge, MA, 02138, USA
[+]Dr. R. V. Martinez and Dr. A. B. Subramaniam contributed equally to this work.

DOI: 10.1002/adfm.201300780

surface tensions than paper surfaces treated with non-fluorinated alkyl trichlorosilanes ("non-fluorinated paper", or "R^H paper"), even though both fluorinated and non-fluorinated paper surfaces exhibited similar contact angles with water ($\theta_{app}{}^{H_2O}$>140°, where $\theta_{app}{}^{H_2O}$ is the apparent static contact angle of water on the modified paper). The combined effects of the long fluoroalkyl chains of grafted siloxane molecules with the micro-scale roughness and porosity of paper (the papers used in this study have a 45–78% void volume fraction), yield an omniphobic material that preserves the properties of mechanical flexibility and low resistance to transport of gas of the untreated paper.

2. Background

We and others have used a variety of techniques to minimize the tendency of paper to adsorb liquids (reviewed here.[22–28]) Methods to render paper hydrophobic include spraying alcohol suspensions of SiO_2 nanoparticles on surface of the paper,[29] soaking in polystyrene solutions,[30] patterning using photolithography with SU-8,[10] wax printing,[9] plasma processing,[31] and treatment with silanizing reagents.[8,32–35]

Organosilanes with hydrophobic organic groups have been used to make the hydrophilic hydroxyl-rich surfaces of cellulose-based materials hydrophobic following both gas-phase[33,34,36,37] and solution immersion reactions.[34,38–40] Most methods, however, require long reaction and processing times (usually longer than one hour[33,34]) and immersion in solvents requires pre- or post-treatment steps (washing cycles to remove excess reagents or side products, drying, etc.); these processes typically produce surfaces that have limited hydrolytic stability,[41] or limited repellency to liquids with surface tensions lower than that of water.[33] They also often cause the paper to buckle or warp.

The method we describe transforms paper into an omniphobic material by exposure to vapors of a fluoroalkyl trichlorosilane; it is simple (single step), rapid (~5 min to completion), and low-cost. We estimate a cost for the materials required for the transformation of hydrophilic paper into an omniphobic material to be less than \$0.8 m^{-2} (for materials purchased on a small scale, as research reagents). We characterized the wetting behavior of the R^F paper, and used it to fabricate functional paper-based devices: microtiter plates able to contain polar and non-polar solvents, and gas sensors, both constructed using the principles of origami.[42]

Part of the oleophobicity of organosilane-functionalized paper reflects its textured surface: a mixture of small fibers (~20 μm in diameter, by scanning electron microscopy (SEM)) and voids (5–100 μm in diameter, by SEM). This textured surface enables it to form metastable composite solid-liquid-air interfaces. This architecture—one comprising voids and solid structures—is the basis of other hydrophobic and omniphobic surfaces[43] and is part of the well-studied lotus leaf effect.[44] Aizenberg et al., and more recently others, have extended this type of structure to sub-micron pillars—etched[45] or molded into a solid support.[46]

A different biomimetic architecture inspired by the *Nepenthes* pitcher plant involves the formation of an immobilized film of a low surface tension liquid at the "solid"-air or "solid"-liquid interface; this structure nearly eliminates pinning of the contact line for both high- and low-surface-tension liquids, and leads to a remarkably low contact angle hysteresis. Based on this principle, the Aizenberg group created omni.hobic "slippery" surfaces (SLIPS) from low surface energy porous microstructured solid substrates, such as Teflon membranes or arrays of nanoposts functionalized with polyfluoroalkyl silanes, by infusing them with a perfluorinated oil.[47] Following this lead, we further increased the ability of R^F paper to resist wetting by low surface tension liquids (<15 mN m^{-1}), by infusing R^F paper with perfluorinated oils. Paper SLIPS have the advantage of being mechanically flexible, and thus can be folded into three-dimensional structures to serve as elementary flow switches and channels for guided transport of drops of liquid.

3. Results and Discussion

3.1. Fabrication of R^F Paper via Silanization

We used Whatman chromatography paper as the starting material because it is uniform in structure and free of hydrophobic binders or coatings that could interfere with, or mask, the effect of silanization. We chose three types of papers: Whatman Gel Blot paper, Whatman #1 paper, and Whatman #50 paper (see **Figure 1**c

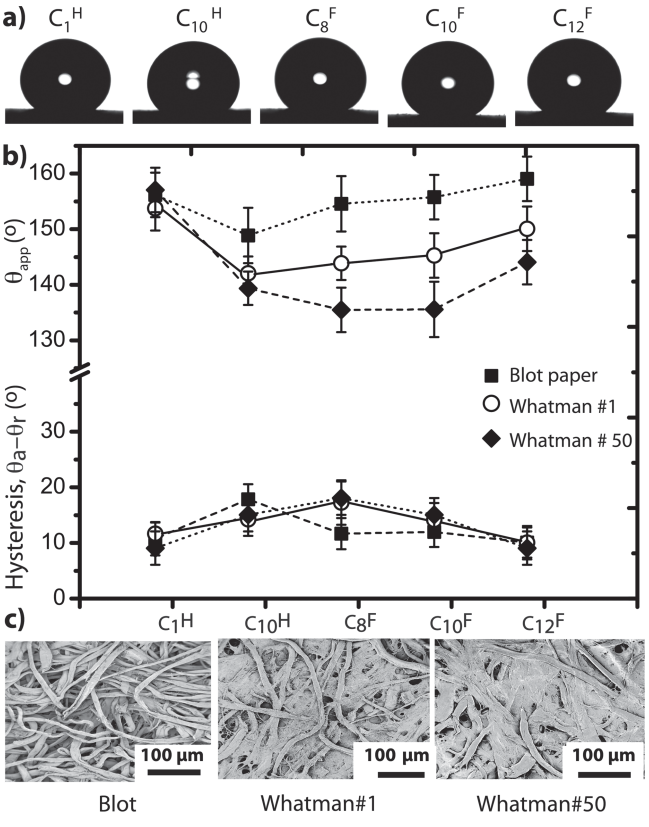

Figure 1. a) Representative images of water droplets on silanized paper. b) Static contact angles (θ_{app}), and contact angle hysteresis (θ_a-θ_r) of water on silanized paper for three types of paper with different surface functionalization. Filled squares represent angles with Gel Blot paper (Blot), hollow circles represent angles with Whatman#1 paper (W1), and filled diamonds represent angles with Whatman #50 paper (W50). The volume of each drop is 10 μL. Error bars: standard deviations for N = 30 measurements. c) SEM images showing the topography of the different paper surfaces.

for SEM images). Visually and by touch, Whatman #50 paper seemed the smoothest, followed by Whatman #1, while Whatman Gel Blot paper felt the roughest. We used optical profilometry to characterize the root mean square roughness—the standard deviation of the surface height distribution—of the papers, because it is more sensitive to large deviations from the mean line than other statistical measurements of roughness.[48] The profile root mean square roughness parameter, $R_{R.M.S.}$, of these papers, was 9.6 ± 2.0 μm for Gel Blot paper, 6.4 ± 1.9 μm for Whatman #1 paper, and 3.3 ± 1.2 μm for Whatman #50 paper. The area root mean square roughness parameter,[49,50] $S_{R.M.S.}$, was 13.5 ± 0.7 μm for Whatman Gel Blot paper, 10.7 ± 0.6 μm for Whatman #1 paper, and 6.5 ± 0.3 μm for Whatman #50 paper. The texture aspect ratio, an indicator of surface isotropy based on the autocorrelation image, varied between 61% for Whatman Gel Blot paper, 45% for Whatman #1, and 37% for Whatman #50 paper (see Supporting Information for details). The roughness anisotropy index, $A_{R.M.S}$, defined as the ratio of $R_{R.M.S.}$ values measured along the x and y axes of the machine,[48] varied for each paper, from about 1.4 for Whatman #50, to 1.2 for Whatman#1 and to 1.1 for Whatman Gel Blot paper (see Supporting Information for details). The porosity, or the volume fraction of void, was measured to be ~78% for Whatman Gel Blot paper, ~68% for Whatman #1 paper, and ~45% for Whatman #50 paper (see Supporting Information and Table S3 for details).

We chose gas-phase silanization to render paper hydrophobic because the procedure does not require pre- or post-treatment steps and the processing can be completed within minutes. We believe this method, with development, is scalable and compatible with large-scale processing (that is, it will be able to generate virtually unlimited areas of silanized paper, using a standard reel-to-reel processing technique).

We used five commercially available organosilane reagents ($RSiCl_3$), in order to study the effect of chain length and fluorination of the organosilane on the wettability of paper: i) methyltricholorosilane (CH_3SiCl_3, "C_1^H"); ii) decyltrichlorosilane ($CH_3(CH_2)_9SiCl_3$, "C_{10}^H"); iii) (3,3,4,4,5,5,6,6,7,7,8,8,8-tridecafluorooctyl) trichlorosilane ($CF_3(CF_2)_5CH_2CH_2SiCl_3$, "$C_8^F$"); iv) (3,3,4,4,5,5,6,6,7,7,8,8,9,9,10,10,10-heptadecafluorodecyl) trichlorosilane ($CF_3(CF_2)_7CH_2CH_2SiCl_3$, "$C_{10}^F$") ; v) (3,3,4,4,5,5,6,6, 7,7,8,8,9,9,10,10, 11,11,12,12,12-henicosafluorododecyl) trichlorosilane ($CF_3(CF_2)_9CH_2CH_2SiCl_3$, "$C_{12}^F$"); C_{12}^F is the trichlorosilane with the longest fluorinated alkyl chain that is currently commercially available.

The silanization reaction was performed in a vacuum oven at 95 °C and 30 mbar using a solution of the organosilane (~10 mL of a ~30 mm solution in toluene) to supply a useful concentration of the silanizing reagent in the vapor phase. The organosilane was allowed to react with the hydroxyl-rich cellulose paper surfaces for 5 min (this time and temperature are not optimized). This process makes it possible to functionalize the areas of paper (>100 cm^2) required for experimental work rapidly, using low quantities of organosilane and solvent.

3.2. Characterization of the Wettability of Silanized Paper

We examined, by means of apparent static (θ_{app}), advancing (θ_a), and receding (θ_r) contact angle measurements, the wettability of paper substrates modified by gas-phase silanization by a wide range of liquids: organic liquids with different surface tensions, biological fluids, and aqueous solutions of ionic and non-ionic surfactants above the critical micelle concentration (cmc). In addition, we tested the compatibility of the different silanized papers with buffers relevant for immunoassays,[51–53] electrophoresis,[54–56] magnetic levitation,[57] polymerase chain reactions (PCR),[58,59] and culture of mammalian cells[60,61] or bacteria.[62]

To ensure that the shape of the droplet is determined by surface forces and is not due to gravitational deformation, we used 10 μL droplets of liquid for the contact angle measurements, to ensure that the radii of the droplets fall below the capillary length. For a liquid of density ρ and surface tension γ_{LV}, the capillary length λ_c is:

$$\lambda_c = \sqrt{\frac{\gamma_{LV}}{\rho g}} \quad (1)$$

For the liquids we selected, λ_c ranged between 1.6 mm (for pentane) and 2.7 mm (for water), higher than the radii of the droplets we used in our measurements (radii of ~1.4 mm). Figures S2 and S3 show optical profilometry images of areas of the papers we have used in our study, illustrating the relevant variations of paper topography at a scale in the same order of magnitude as the droplet size (mm). This suggests that local variations in the topography of the paper may induce some variation in the angle measurement and might be partially responsible for the dispersion that we observe in our contact angle data.

Paper is known to be anisotropic.[48,63] For our contact angle measurements, we did not maintain a specific orientation of the paper. The paper was cut into small strips along random axes, placed into a sample box, and retrieved randomly for the contact angle measurements. Thus, the contact angles of the liquids that we measured are presumably an average over all orientations of the paper.

3.3. Treatment of Paper with an Organosilane (either R^HSiCl_3 or R^FSiCl_3) in the Vapor Phase Renders Paper Highly Repellent to Pure Water

Figure 1a and Supporting Movie M1 show that silanization rendered paper highly hydrophobic; water no longer wicked into the paper, but instead formed droplets on the surface with apparent static contact angles, θ_{app}, between 130° and 160°, and with contact angle hysteresis from 7° to 20°. The apparent contact angle of each type of functionalized paper increased (modestly) for the most part with the chain length and degree of fluorination of the organosilane, while the hysteresis did not show any noticeable trends (Figure 1b).

The equilibrium contact angle, θ_Y, that a liquid forms on a chemically homogeneous, smooth solid surface is given by the Young's equation Equation (2), where γ_{SV} is the solid/vapor surface free energy per unit area, γ_{SL} is the solid/liquid surface free energy per unit area, and γ_{LV} is the liquid/vapor surface free energy per unit area:[64]

$$\cos\theta_Y = \frac{\gamma_{SV} - \gamma_{SL}}{\gamma_{LV}} \quad (2)$$

From Equation (2) it is apparent that water will form a higher contact angle on surfaces with lower surface free energy, i.e., lower γ_{SV} (even on rough hydrophobic surfaces.[64] Thus, our results can be rationalized, assuming approximately equal grafting densities of the organosilanes on paper, by noting that (i) trifluoromethyl and difluoromethylene groups have a lower energy than methyl and methylene groups,[64] respectively, that (ii) longer chains lead to more efficient packing of the organosilanes on the surface of the paper, exposing a higher ratio of trifluoromethyl: difluoromethylene or methyl: methylene groups,[64] and (iii) longer chains of fluorinated organosilanes lead more fluorine groups on the surface of the paper. Paper functionalized with methyltrichlorosilane, however, consistently exhibited higher static contact angles than what would have been predicted from the properties of the grafted methyl group (Figure 1b). The literature reports that methyltrichlorosilanes can polymerize and form nanoscale three-dimensional features such as cross-linked nanofibers[65] or nanospheres.[33,65] On the paper surface, such polymerized features would result in a grafting density of methyl siloxanes that is higher than the grafting density of the longer alkyl siloxanes, and could also lead to changes in the topography of the surface.

Since paper is composed of a mesh of partially oriented cellulose fibers, wetting of liquids on its surface is not only dictated by the surface free energy per unit area, but also by the topography of the surface.[64] To account for the topography, Equation (2) must be modified appropriately. Two models of wetting on "rough" surfaces are widely used, (i) the Wenzel model for homogeneous wetting, with the liquid following the topography of the surface, and (ii) the Cassie-Baxter model, with the liquid droplets exhibiting composite, heterogeneous wetting with air pockets trapped between protruding topographical features.[64]

In the Wenzel model,[66] the apparent contact angle that a liquid droplet makes on the rough surface is given by Equation (3), where r is the non-dimensional substrate "roughness", defined as the ratio of the real surface area to the apparent (projected) area; $r = 1$ for a smooth surface and $r > 1$ for a rough surface.

$$\cos\theta_{app} = r\cos\theta_Y \tag{3}$$

When the liquid droplet exhibits composite wetting, i.e., the area wetted consists of liquid–solid contacts and liquid–air contacts (the air being trapped between the troughs of the rough surface) the Cassie-Baxter model, described by Equation (4), is applicable. Here f_1 is the area fraction of the liquid interface in contact with the solid and $f_2 = 1–f_1$ is the area fraction of the droplet in contact with the air trapped between troughs.

$$\cos\theta_{app} = rf_1\cos\theta_Y - f_2 \tag{4}$$

In both models, increasing r leads to a higher apparent contact angle for hydrophobic ($\theta_Y > 90°$) surfaces. The geometric parameter r, however, depends not only on the topography but also on the local contact angle that the liquid makes on the surface features.[43] We use the profile root mean square roughness parameter ($R_{R.M.S.}$) as a surrogate for r. Indeed, our data show that water forms droplets with higher apparent contact angles on surfaces with higher $R_{R.M.S.}$ (Figure 1). The contact angle data of methyltrichlorosilane (C_1^H)-treated paper did not follow the trend, and showed no measurable difference between the

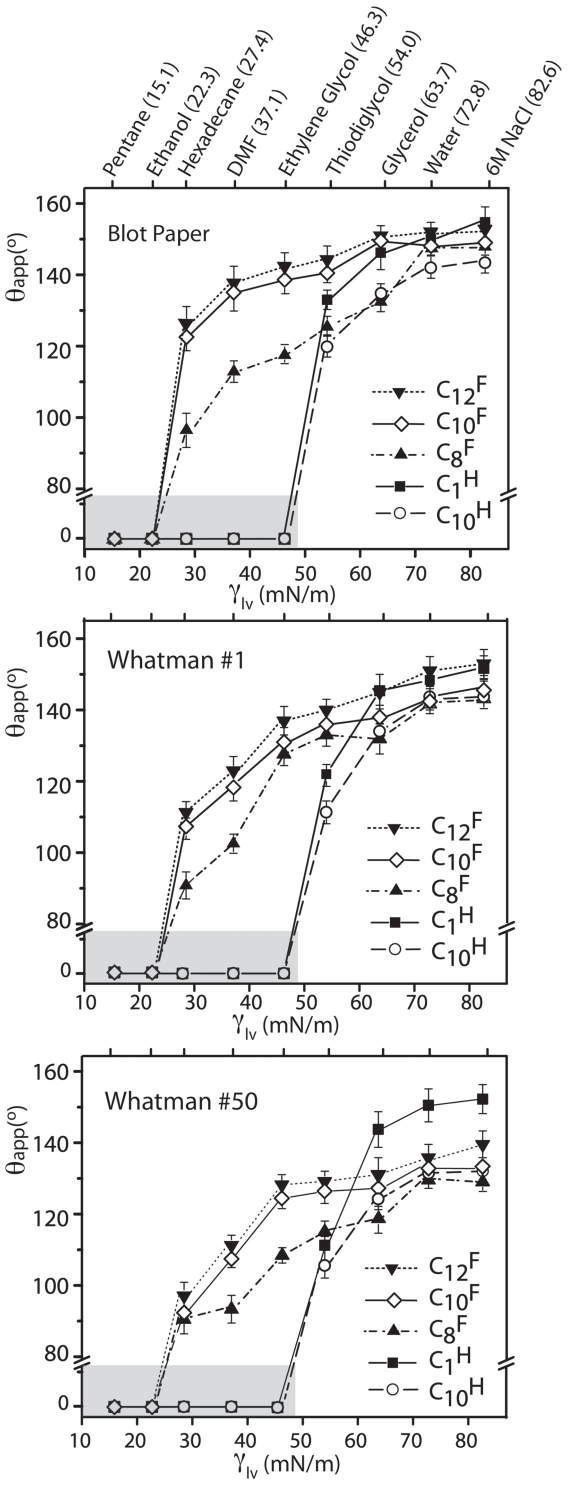

Figure 2. The dependence of static contact angles on surface tension for 10 µL droplets of liquid. The liquids used in these experiments and their respective surface tensions (γ_{LV}) at 20 °C in mN m^{-1} are (literature values[63]): pentane (15.5), anhydrous ethanol (22.3), hexadecane (27.4), dimethylformamide (DMF) (37.1), ethylene glycol (46.3), thiodiglycol (54.0), glycerol (63.7), water (72.8), a 6 M aqueous solution of NaCl (82.6). Error bars: standard deviation for N = 30 measurements. The grey area indicates liquids that spontaneously spread onto the substrate through capillary wicking.

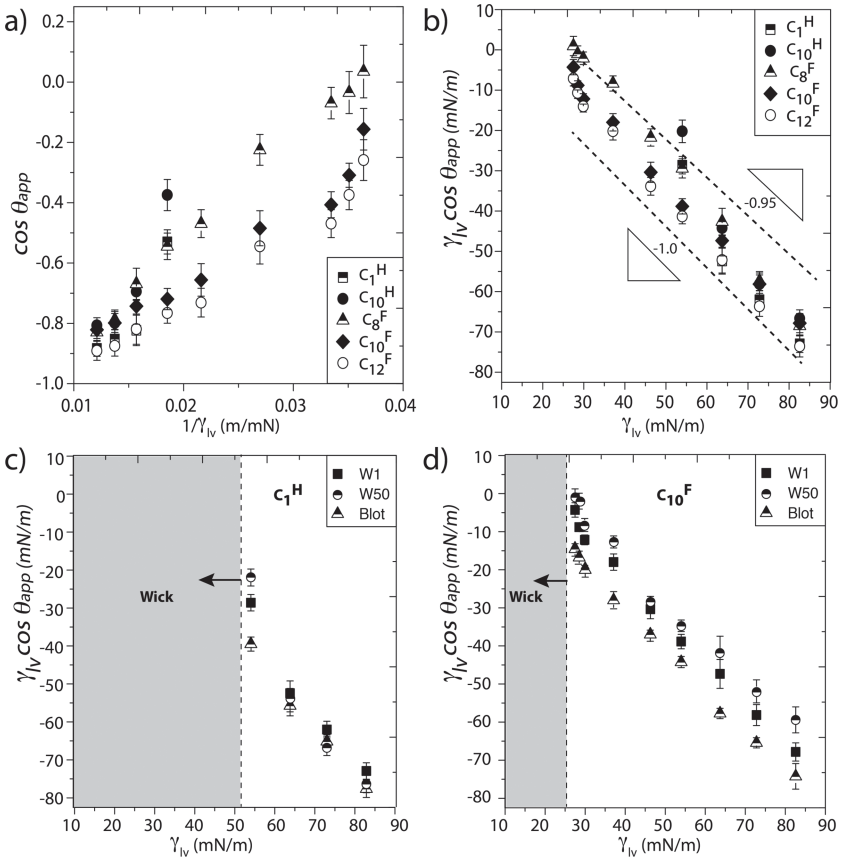

Figure 3. Analysis of liquid contact angle data on silanized paper. a) Plot of *cos* θ_{app} versus $1/\gamma_{LV}$ for the five silanes of differing chain lengths and degree of fluorination on Whatman #1 paper. b) Plot of γ_{LV} *cos* θ_{app} versus γ_{LV} for the five silanes of differing chain lengths and degree of fluorination on Whatman #1 paper. The data collapses onto straight lines, indicative of Cassie-Baxter type wetting, with slopes in the range of –1.0 and –0.95. These values indicate that a large area fraction of the droplets is resting on air. c) Plot of γ_{LV} *cos* θ_{app} versus γ_{LV} for three different types of paper, each treated indistinguishably with C_1^H silane. d) Plot of γ_{LV} *cos* θ_{app} versus γ_{LV} for three different types of paper each treated indistinguishably with C_{10}^F silane. For the three types of paper we analyzed, topography appears to have a smaller effect on liquid repellency than the degree of fluorination of the organosilane.

different types of paper. One possible explanation for this behavior is the formation of nanostructures[33,65] on the surface of the cellulose fibers in C_1^H-treated paper.

3.4. R^F Paper Repels a Wider Variety of Liquids Than R^H Paper

Many applications involve contact of surfaces with liquids that have lower surface tensions than water. To determine the compatibility of silanized paper with organic liquids, we measured the contact angles of nine test liquids with liquid–air interfacial tensions that range from 16 and 83 mN m^{-1} on silanized paper (surface tensions obtained from tabulated values in the literature).[67]

R^H paper was able to resist wetting by liquids with surface tensions >54 mN m^{-1} (thiodiglycol; $(HOCH_2CH_2)_2S$). Test liquids with lower surface tensions wicked into the paper. R^F paper was able to resist wetting by liquids with surface tensions as low as 27 mN m^{-1} (hexadecane) (**Figure 2** and Supporting Information, Figure S4). This value likely reflects the lower energy of the paper fibers functionalized with fluoroalkyl siloxane chains[64] relative to those functionalized with alkyl siloxanes.

In order to interpret our data in terms of the variable under our control (the surface tension of the test liquids, γ_{LV}) and the variable that we measure (the apparent contact angle, θ_{app}), we expressed Equations (3) and (4) in terms of surface tensions expressed in Equation (2).

$$\cos\theta_{app} = \frac{1}{\gamma_{LV}} r\,(\gamma_{SV} - \gamma_{SL}) \quad (5)$$

$$\gamma_{LV}\cos\theta_{app} = -f_2\gamma_{LV} + rf_1\,(\gamma_{SV} - \gamma_{SL}) \quad (6)$$

We plot *cos* θ_{app} versus $1/\gamma_{LV}$ for the various organosilanes on Whatman #1 paper (**Figure 3**a). Based on Equation 5, we expect our contact angle data to collapse to straight lines with zero intercepts, if the wetting of liquids followed the Wenzel model on silanized paper.

Figure 3a clearly demonstrates that the wetting behavior of liquids on silanized paper deviates significantly from the Wenzel model. When γ_{LV} *cos* θ_{app} is plotted versus γ_{LV}, we find that our data for silanized Whatman #1 paper collapses onto straight lines with negative slopes (Figure 3b), a behavior qualitatively consistent with Equation (6). The data for all the organosilanes tested fall within straight lines with slopes of –1 and –0.95 (i.e., f_2~ between 1 and 0.95). This behavior suggests that the surface of the droplets primarily contacts the air pockets trapped at the interface with the paper surface. Similar behavior was observed for Whatman #50 and Gel Blot papers (data not shown).

To illustrate the effect of topography on the wettability of the papers, Figure 3c,d shows contact angle data plotted for two types of silanization, C_1^H and C_{10}^F on the three different types of paper. Within the range of topographies we tested, liquids behave in a manner that is consistent with the Cassie-Baxter model. There is a clear and systematic deviation from the linear trend of the contact angle data as the surface tension of the test liquids approached the wicking transition of the silanized papers. The deviation is present for all organosilane derivatives and for all types of paper tested (Figure 3c,d). We speculate that this deviation close to the wicking transition suggests a mode of wetting different from the classical Cassie-Baxter model, and would be an interesting phenomenon to investigate in the future.

3.5. R^F Paper is Superior to R^H Paper for Applications Requiring Minimal Interactions with Biological Fluids

The wetting of silanized paper by biological fluids is important for its use in applications such as bioanalysis, cell culture, and

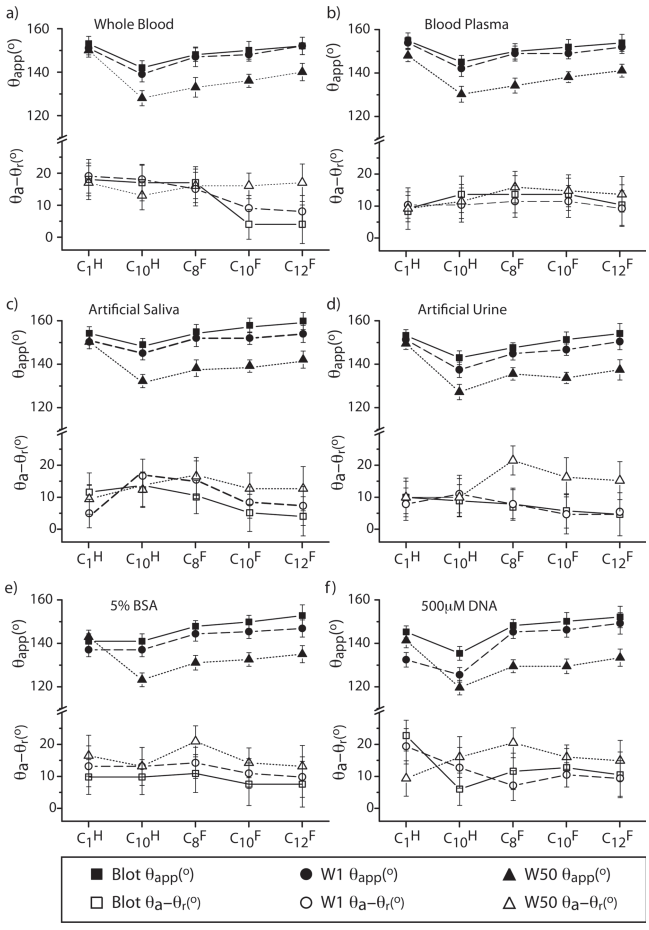

Figure 4. Static contact angles (filled symbols) and hysteresis (θ_a-θ_r) (hollow symbols) of several biological fluids: a) whole blood, b) plasma, c) artificial saliva, d) artificial urine, e) a solution of protein (5% BSA in PBS), and f) a solution of DNA (500 μM of DNA in TE buffer) on functionalized Gel Blot (square symbols), Whatman #1 (circular symbols) and Whatman #50 (triangular symbols). Error bars: standard deviation for N = 30 measurements.

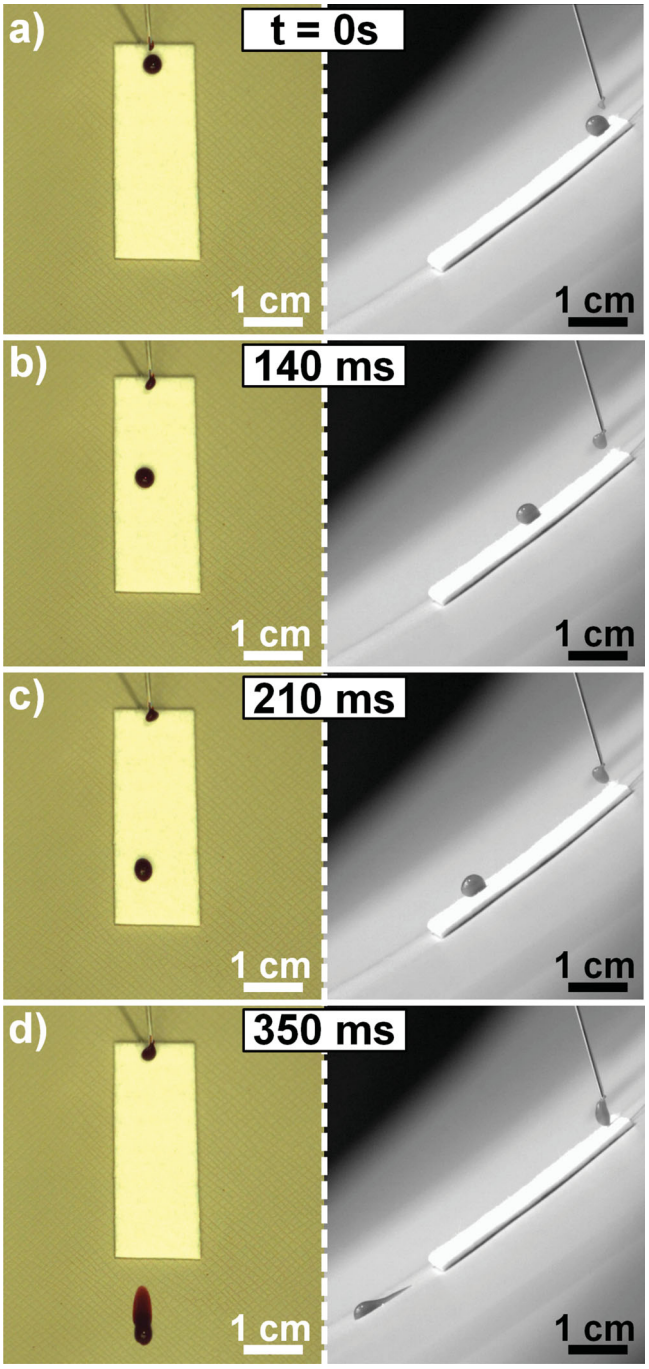

Figure 5. Time-sequence images of a drop of heparinized human blood rolling down on Gel Blot paper functionalized with C_{10}^F (side view: right; front view: left). The tilting angle is 30°. The rolling drop does not leave a stain visible to the unaided eye (see also Supporting Movie M2).

drug discovery and development. Viscous solutions with a high content of protein or DNA, such as artificial saliva, a 5% (mass-to-mass ratio) solution of bovine serum albumin (BSA) in PBS, and a 500 μm solution of DNA in Tris-EDTA (TE) buffer, formed higher contact angles on fluorinated than on non-fluorinated papers of corresponding roughness (**Figure 4**c–f). In all cases, the longer the fluorinated alkyl chains, the higher the static contact angle.

Whole blood (fresh whole human blood treated with an anticoagulant-preservative solution containing sodium heparin, supplied by Research Blood Components, LLC.) and plasma (supplied by Research Blood Components, LLC.) formed contact angles larger than 150° on both R^H and R^F papers. Droplets of whole blood and plasma exhibit the lowest contact angle hysteresis (<15°) with fluorinated surfaces (Figure 4a,b). A drop of whole blood rolling on the surface of a strip of paper functionalized with C_{10}^F, and C_{12}^F did not leave a visible trace behind (**Figure 5** and Supporting Movie M2). The lack of staining is reminiscent of the behavior of the "slippery" omniphobic surfaces fabricated by the Aizenberg group,[47] and suggests a low level of cell and protein adhesion on the R^F paper, following very brief (on the order of several seconds) contact with biological fluids. The effect of long-term contact of R^F paper with biological fluids is beyond the scope of this article.

For applications involving blood, it might be important to minimize the amount of trace liquid left behind on the surface

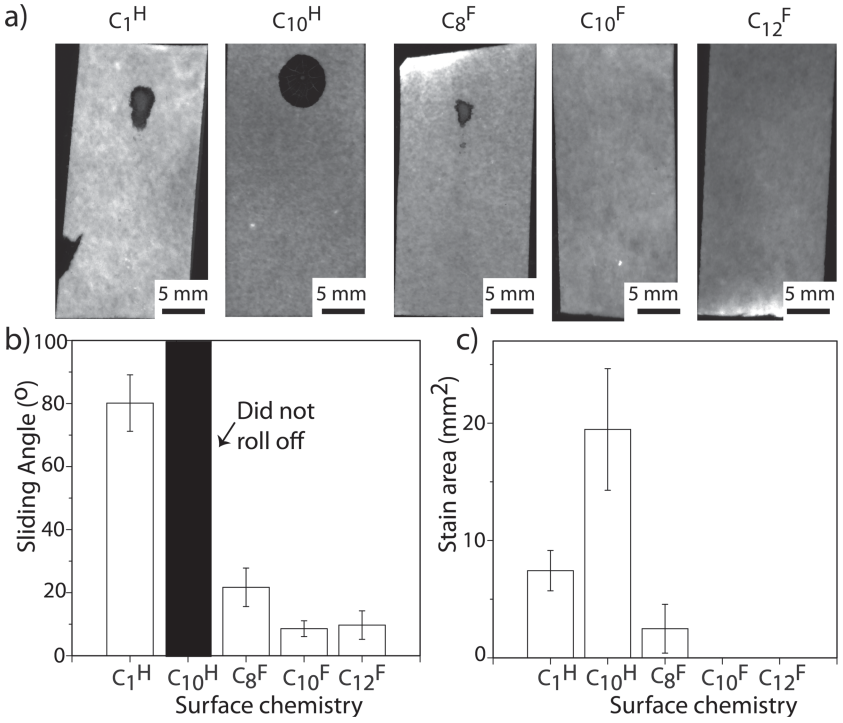

Figure 6. a) Images obtained with a fluorescence gel scanner from silanized paper after the drop of blood released and rolled off on tilted paper. The dark spots are dried blood. b) The angles of incline at which the droplets of blood rolled off the silanized papers. c) The amount of blood adhering to the paper after the blood droplet had rolled off, quantified as the area of the blood stain left on the paper. Bars are standard deviations for N = 7 measurements.

(i.e. the surface should be self-cleaning). To test the performance of silanized paper and quantify the behavior observed in Figure 5 and Supporting Movie M2, we deposited 50 μL drops of blood on the surface of various silanized papers that were initially horizontal. We then increased the tilt angle until the drop of blood rolled off the surface of the paper. **Figure 6**a shows representative images of the paper surfaces after the blood had rolled off. There are significantly more traces of blood left on the R^H papers than on the R^F papers. Papers treated with the organosilanes with the longer fluoroalkyl chains ($C_{10}F$ and $C_{12}F$) showed no detectable trace of blood on the surface after roll-off. Figure 6b shows the roll-off angles measured for these papers. R^H papers had significantly higher roll-off angles than R^F papers. The blood drops adhered so strongly to $C_{10}H$ treated surfaces that the droplets did not fall off even when the paper was turned upside down. The state characterized by high adhesion and high contact angles has been termed the "petal effect"[68] and is attributed to hierarchical roughness (multiple length scales of features) on surfaces.

3.6. Products Formed upon Incineration of R^F Paper

Bioanalytical devices fabricated using silanized paper can be disposed of by incineration; we wished to estimate the environmental impact of burning R^F paper. The elemental analysis of the fluorinated papers, suggests that the incineration of a 1 cm^2 device at T < 1500 °C can produce at most 34 μg of a perfluoroalkyl carboxylic acid; under more stringent conditions (temperatures above 1500 °C), this content of fluorine could lead to the formation of a maximum of ca. 29 μg of HF, or a maximum of ca. 49 μg of COF_2.

3.7. R^F Paper is Compatible with Buffers Commonly Used in Bioassays

We surveyed the wettability of silanized paper by common buffers, since the surface tension of an aqueous buffer can be dramatically altered by the addition of surfactants or other solutes. The buffers we surveyed include PBS, Tris, Taq Buffer (used for polymerase chain reactions), Tris-Gly buffer (typically used in capillary electrophoresis); Lysogeny broth (LB) or Dulbecco's Modified Eagle Medium (DMEM)—buffers typically used for mammalian or bacterial cell culture. Buffers containing amines, amino acids, or dissolved salts form contact angles that are indistinguishable from that formed by pure water (Supporting Information, Figure S5).

An important distinction between the R^F and R^H surfaces however, is in their ability to resist wetting by aqueous solutions of nonionic surfactants. These surfactants reduce the surface tension of pure water to ~30 mN m^{-1} when present at or above the critical micelle concentration (cmc).[69] Nonionic surfactants are present in standard buffers used for PCR reactions, such as the Taq Buffer. When used above the cmc, nonionic surfactants containing polyethylene oxide chains, (e.g. IGEPAL CA@630, Triton X-100, and Tween 20), wetted R^H, but not the R^F paper surfaces (Supporting Information, Figure S6). Therefore, R^H papers are not compatible with applications that require buffers containing nonionic surfactants.

3.8. Fabrication of Functional 3D Omniphobic Structures by Simple Creasing and Folding of R^F Paper

Gas-phase silanization does not affect the mechanical properties of the paper substrate. Thus, three-dimensional functional structures can be built by creasing or folding the paper, either before or after silanization. We took advantage of the mechanical flexibility and foldability of the R^F paper to create microtiter plates from single sheets of paper using the principles of origami.[42] Two different designs were used for fabricating the microtiter plates: a square array of re-entrant honeycomb cells (**Figure 7**a), and a negative Poisson ratio structure based on a triangular array of re-entrant honeycomb cells[70] (Figure 7c). Figure 7 shows microtiter plates made from R^F paper holding an aqueous solution (DMEM, Figure 7b) and an organic liquid (toluene dyed with Sudan I, Figure 7d). The R^F paper structures formed stable walls that contained both liquids, without wicking, cracking or collapsing, for a period of 14 days (which

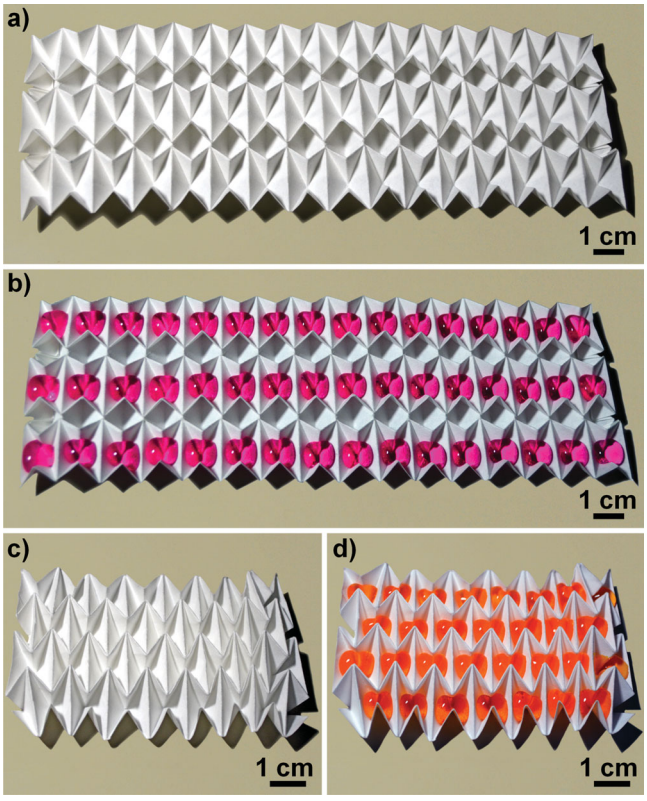

Figure 7. Omniphobic microtiter plates fabricated by creasing and folding of R^F paper: a) a square array of re-entrant honeycomb cells, and c) a negative Poisson ratio structure based on a triangular array of re-entrant honeycomb cells. These structures are able to stably hold in each well 500 µL of b) aqueous solutions (DMEM) and d) organic liquids (toluene dyed with Sudan I).

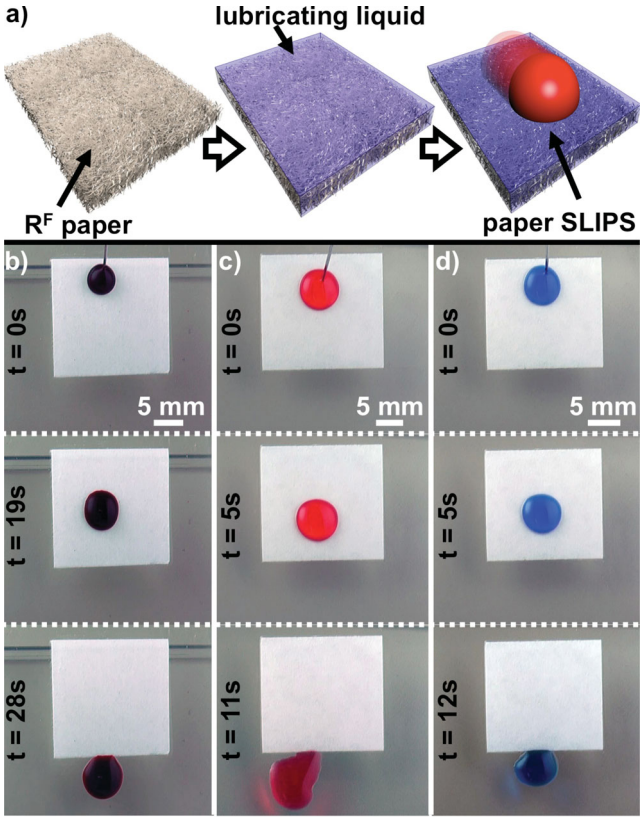

Figure 8. a) Fabrication of paper slippery porous liquid-infused surfaces (paper SLIPS) from R^F paper impregnated with a perfluoropolyether. Time-sequence images showing sliding droplets of: b) heparinized human blood (volume ~ 30 µL), c) diethyl ether dyed with Sudan Red (γ_{LV} = 17 mN m^{-1}, volume ~ 30 µL) and d) toluene dyed with Sudan Blue (γ_{LV} = 28 mN m^{-1}, volume ~ 30 µL) on a paper SLIPS at ~5° tilting (see Supporting Movies M3, M4, and M5).

is simply the duration of our observation of the system). Under our experimental conditions, we did not observe a difference in the stability of structures fabricated by folding paper either before or after silanization (data not shown).

3.9. R^F Paper Infused with a Perfluorinated Liquid forms an Omniphobic "SLIPS" Surface Exhibiting Very Low Contact Angle Hysteresis

We introduced perfluoropolyether lubricant (Dupont Krytox GPL 105) onto R^F paper surfaces. The liquid spontaneously spreads onto the whole substrate through capillary wicking, and the large pores in paper facilitate the infiltration and retention of the lubricating perfluoropolyether to form a continuous overlying film. **Figure 8** shows how R^F paper can serve as a substrate for SLIPS—"Slippery Liquid-infused Porous Substrates" with remarkably low hysteresis towards most liquids.[47,71,72] Blood, toluene, and diethyl ether all slide off the paper SLIPS when the surface is tilted at a 5° angle (Supporting Movies M3, M4, and M5).

Figure 9a demonstrates that paper SLIPS show omniphobic behavior, with contact-angle hysteresis of the surface below 10° for all liquids we tested, and below 5° for most of them. Paper SLIPS are also able to resist wetting by n-pentane, which has a surface tension of ~15 mN m^{-1}. Since the wetting characteristics (apparent contact angles, θ_{app}, and hysteresis, $\theta_a - \theta_r$) of the paper SLIPS did not vary for the three types of paper substrates, we hypothesized that the film of perfluoropolyether oil dominates the wetting characteristics of this material.

To test this hypothesis, we measured the surface tension of the perfluoropolyether oil and the liquid–liquid interfacial tension between the perfluoropolyether oil and the test liquids using the pendant drop method. These values, along with the liquid–air surface tensions, provide all three surface energy components for calculating the equilibrium contact angle, θ_Y, of our test liquids resting on a hypothetical smooth, solid surface that consisted only of the perfluoropolyether oil. We plot $cos\ \theta_Y$, calculated using Equation (2) versus the $cos\ \theta_{app}$ in Figure 9b, and find that indeed these values are strongly correlated. Thus, the wetting behavior of paper SLIPS can be reasonably predicted from the interfacial tension of a liquid of interest with the lubricating oil with Young's equation.

A useful feature of paper SLIPS is their foldability, which can be exploited for low-cost fabrication of structures with desired functionalities. Complex 3D "slippery" structures of paper SLIPS

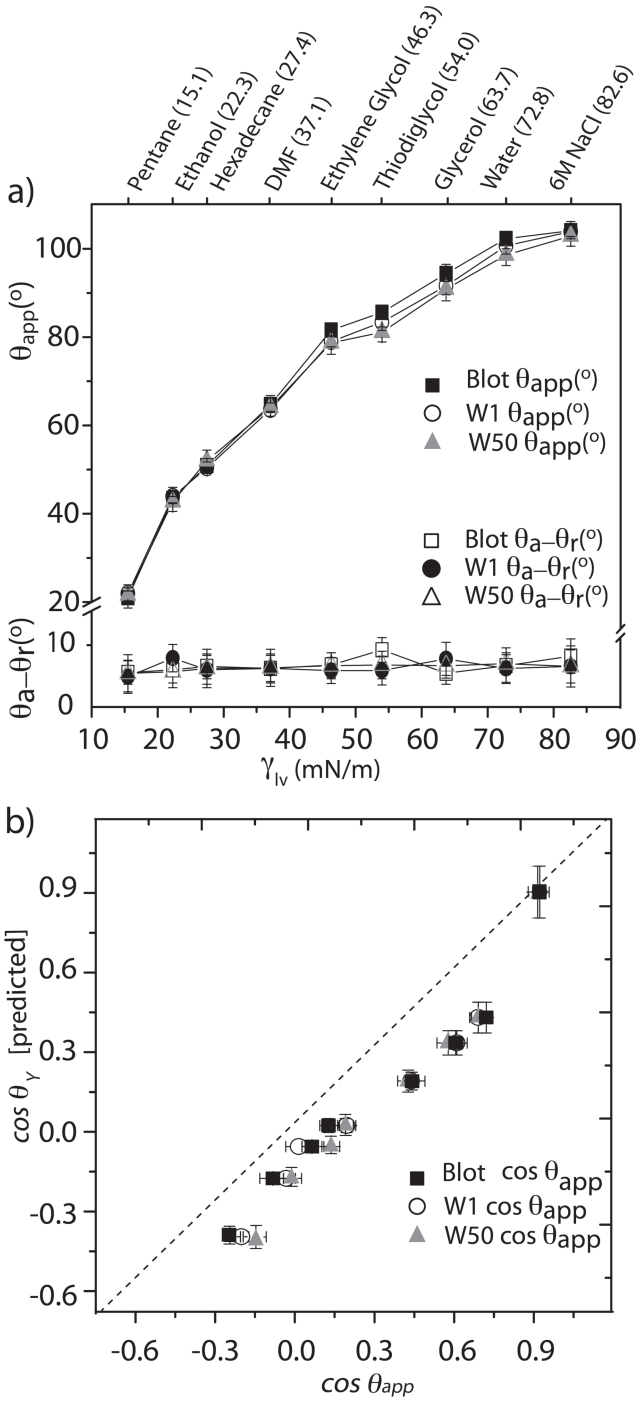

Figure 9. a) Comparison of apparent contact angles and contact angle hysteresis (θ_a-θ_r) as a function of surface tension of test liquids (indicated) for SLIPS fabricated from Gel Blot, Whatman #1 and Whatman #50 paper silanized with C_{10}^F and impregnated with a perfluoropolyether lubricant (Dupont Krytox GPL 105). b) Plot of the cosine of the predicted equilibrium contact angle—calculated with the assumption that the liquids wet a hypothetical flat surface composed solely of perfluoropolyether lubricant—versus the cosine of the measured apparent angle of liquids with the paper SLIPS. The diagonal dashed line is drawn to guide the eye to show the case of perfect correlation.

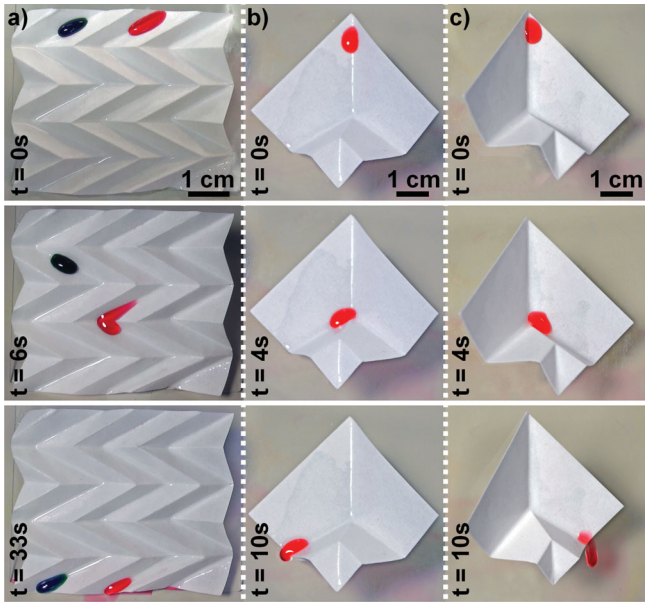

Figure 10. 3D "slippery" structures fabricated by folding and creasing R^F paper impregnated with a perfluoropolyether lubricant (Krytox GPL105). The paper was first impregnated, and then creased. These structures can guide the transport of liquid droplets of dyed methanol (green) and dyed toluene (red) using a) a slippery "channel" formed by successive V-pleats in a paper SLIPS (see Supporting Movie M6) or b,c) a fluidic switch formed by combining tilting and a pre-defined geometry.

can be easily fabricated using techniques based on (for example) origami directly from paper SLIPS, or from R^F paper folded, then impregnated with a perfluoropolyether. To demonstrate their mechanical flexibility and foldability, we folded paper SLIPS to make V-pleats and form "slippery" channels that can be used to guide droplets of toluene and methanol (**Figure 10**a, and Supporting Movie M6). We created a simple switch by combining tilting with a pre-designed folded geometrical path. When the structure is tilted towards the left, the liquid droplet moves along the left-hand channel (Figure 10b), while when the structure is tilted to the right, the path the liquid droplet takes is changed and the droplet moves along the right-hand channel (Figure 10c). Paper SLIPS thus differ from those prepared by Aizenberg et al. in the ease with which (originally) planar sheets can be transformed into structures with complex topographies by folding.

3.10. Colorimetric Detection of Volatile Compounds Using R^F Paper Devices

R^F paper is repellant to liquids with surface tensions greater than 28 mN m^{-1}; at the same time, it is highly permeable to gases and compounds in the vapor phase. We folded R^F paper to create small (4 cm^3) parallelipipedically-shaped chambers that we used for the colorimetric detection of hydrogen sulfide and volatile primary amines. We contained an aqueous solution of either $CuSO_4$ or picrylsulfonic acid in the chamber and sealed its top with a transparent gas-impermeable tape (Fellowes adhesive sheet, PET/

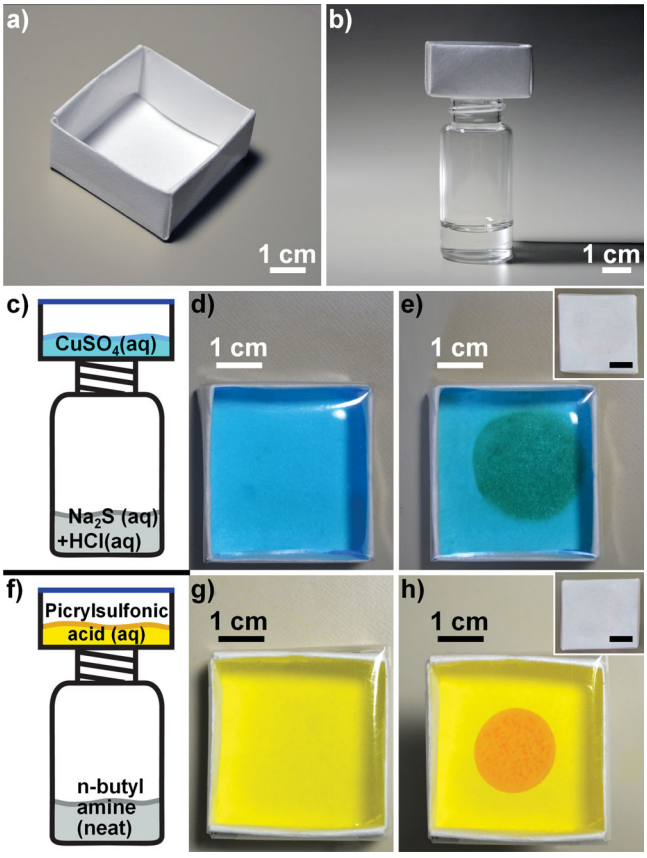

Figure 11. Gas permeable but liquid impermeable "chambers" fabricated by folding and creasing R^F paper and sealing the top with a gas-impermeable tape (Fellowes adhesive sheet, PET/EVA/LDPE) can be used as colorimetric sensors to detect either hydrogen sulfide or volatile primary amines. a) Design of the "chamber" and b) design of the experiment. Each sealed "chamber" contained an aqueous solution of either d) $CuSO_4$ or g) picrylsulfonic acid (1 M in water). When the paper structure is exposed to a volatile source of H_2S or butyl amine, the solution in the "chamber" forms e) a brown precipitate (CuS), or h) an orange product (n-butyl-2,4,6-trinitroaniline). The insets depict the bottom of the chamber after the colorimetric detection occurred.

EVA/LDPE). A vial containing a solution of hydrogen sulfide or butylamine was placed underneath each chamber for 20 s (see **Figure 11**b), to expose the chambers to the vapors of hydrogen sulfide and butyl amine, respectively; this experiment allowed the volatile compound to pass through the bottom wall and react with the solution contained in the R^F paper chamber. The volatile H_2S reacted with $CuSO_4$ to form a brown precipitate (CuS, Figure 11e); n-butylamine reacted with picrylsulfonic acid to form the orange product n-butyl 2,4,6 trinitroaniline (Figure 11h).

4. Conclusions

We show that a rapid, one-step reaction with a fluoroalkyl trichlorosilane in the gas phase transforms cellulose paper into R^F paper, an omniphobic material that is not wetted (θ_{app}> 90°) by water and organic liquids with surface tension as low as 28 mN m^{-1}. Upon impregnation with a perfluoropolyether lubricant, R^F paper forms a slippery material (paper SLIPS) capable of repelling liquids with surface tensions as low as 15 mN m^{-1}. From a fabrication standpoint, cellulose-based paper is commercially available in a variety of forms—with different roughness, porosity, density, thickness, and flexibility—all of which can be converted into omniphobic materials or SLIPS upon appropriate surface functionalization, or upon functionalization and addition of a lubricant, to meet the needs of specific applications.

The potential for low cost for fabrication of R^F paper enables its use in applications that require gas permeable, disposable liquid barrier membranes, with possible uses as toxic gas sensors, membranes for lung-assist devices or fuel cells. We have recently used R^F paper in combination with a craft-cutter to fabricate open-channel microfluidic devices that are able to reproduce low-Reynolds number pressure-driven fluid dynamics, generate droplets and gradients, and carry out gas-phase chemical reactions.[73] R^F paper is more cost effective (~\$0.8 m^{-2} for cost of materials compared to prices of ~\$1500 m^{-2} for Nafion to ~\$29 m^{-2} for Gore-Tex), but also more repellent to water than materials based on ePTFE: the advancing contact angles of water on R^F paper ($\theta_a^{H_2O}$ >150°) are higher than, for example, the contact angles of water on Gore-Tex membranes ($\theta_a^{H_2O}$ = ~ 110°).[74] Unlike other fluoropolymer-based quasi-omniphobic materials, such as SLIPS[43,47,71,75] or omniphobic synthetic textured solids,[43] R^F paper and paper SLIPS are mechanically flexible materials that can be rolled and folded into a range of complex 3D structures with high stiffness and light weight. These materials are, however, susceptible to damage by stretching or cutting.

We believe that the ability to resist wetting by liquids with a wide variety of surface tensions, combined with mechanical flexibility, foldability, light weight, biocompatibility (e.g., lack of wetting by blood), and gas permeability, make R^F paper a valuable new material, and a possible alternative to polymer-, glass-, and silicone-based materials now used as substrates for biomedical and bioanalytical applications, microfluidics, and MEMS.

Supporting Information

Supporting Information is available from the Wiley Online Library or from the author.

Acknowledgements

This work was supported by the Bill and Melinda Gates Foundation under award 51308. Work focusing on microtiter plates was supported by the Department of Energy (ER45852). R.V.M. acknowledges funding by the FP7 People program under the project Marie Curie IOF-275148. We thank Dr. Claudiu Stan and Dr. Barbara Smith for helpful discussions. We thank Jason Tresback and the Center for Nanoscale Systems (CNS) at Harvard University for technical assistance. This work was performed in part at the Center for Nanoscale Systems (CNS), a member of the National Nanotechnology Infrastructure Network (NNIN), which is supported by the National Science Foundation under NSF award no. ECS-0335765. CNS is part of Harvard University.

Received: March 2, 2013
Revised: May 7, 2013
Published online: July 26, 2013

[1] F. Liu, B. Yi, D. Xing, J. Yu, H. Zhang, *J. Membr. Sci.* **2003**, *212*, 213.
[2] H. Kajiwara, T. Hamada, Y. Ichikawa, M. Ishi, I. Yamazaki, *Artif. Organs* **2004**, *28*, 840.
[3] H. K. Inoue, S. Kobayashi, K. Ohbayashi, H. Kohga, M. Nakamura, *J. Neurosurg.* **1994**, *80*, 689.
[4] C. Minale, G. Hollweg, S. Nikol, C. Mittermayer, B. J. Messmer, *Thorac. Cardiovasc. Surg.* **1987**, *35*, 312.
[5] R. Bardini, V. Radicchi, P. Parimbelli, S. M. Tosato, S. Narne, *Ann. Thorac. Surg.* **2003**, *76*, 304.
[6] R. Sreenivasan, E. K. Bassett, D. M. Hoganson, J. P. Vacanti, K. K. Gleason, *Biomaterials* **2011**, *32*, 3883.
[7] K. Esato, B. Eiseman, *J. Thorac. Cardiovasc. Surg.* **1975**, *69*, 690.
[8] X. Liu, M. Mwangi, X. Li, M. O'Brien, G. M. Whitesides, *Lab Chip* **2011**, *11*, 2189.
[9] E. Carrilho, A. W. Martinez, G. M. Whitesides, *Anal. Chem.* **2009**, *81*, 7091.
[10] A. W. Martinez, S. T. Phillips, G. M. Whitesides, E. Carrilho, *Anal. Chem.* **2010**, *82*, 3.
[11] J. M. Zhang, J. Zhang, *Acta. Polym. Sin.* **2010**, 1376.
[12] R. Martins, I. Ferreira, E. Fortunato, *Phys. Status Solidi RRL* **2011**, *5*, 332.
[13] E. Fortunato, N. Correia, P. Barquinha, L. Pereira, G. Goncalves, R. Martins, *IEEE Electr. Device L.* **2008**, *29*, 988.
[14] S. Yun, S.-D. Jang, G.-Y. Yun, J.-H. Kim, J. Kim, *Appl. Phys. Lett.* **2009**, *95*.
[15] J. Kim, S. H. Bae, H. G. Lim, *Smart Mater. Struct.* **2006**, *15*, 889.
[16] S. K. Mahadeva, S. Yun, J. Kim, *J. Intel. Mat. Syst. Str.* **2009**, *20*, 1141.
[17] K. M. Suresha, S. Y. Yang, M. H. Lee, J.-H. Kim, J. Kim, *Compos. Interface* **2008**, *15*, 679.
[18] A. D. Mazzeo, W. B. Kalb, L. Chan, M. G. Killian, J.-F. Bloch, B. A. Mazzeo, G. M. Whitesides, *Adv. Mater.* **2012**, *24*, 2850.
[19] A. C. Siegel, S. T. Phillips, B. J. Wiley, G. M. Whitesides, *Lab Chip* **2009**, *9*, 2775.
[20] R. Derda, S. K. Tang, A. Laromaine, B. Mosadegh, E. Hong, M. Mwangi, A. Mammoto, D. E. Ingber, G. M. Whitesides, *PLoS One* **2011**, *6*, e18940.
[21] A. W. Martinez, S. T. Phillips, B. J. Wiley, M. Gupta, G. M. Whitesides, *Lab Chip* **2008**, *8*, 2146.
[22] E. Malmstrom, A. Carlmark, *Polym. Chem.* **2012**, *3*, 1702.
[23] S. Kalia, A. Dufresne, B. M. Cherian, B. S. Kaith, L. Averous, J. Njuguna, E. Nassiopoulos, *Int. J. Polym. Sci.* **2011**, Article ID 837875.
[24] A. G. Cunha, A. Gandini, *Cellulose* **2010**, *17*, 875.
[25] C. S. R. Freire, A. Gandini, *Cellul. Chem. Technol.* **2006**, *40*, 691.
[26] H. A. Schuyten, J. D. Reid, J. W. Weaver, J. G. Frick, *Text. Res. J.* **1948**, *18*, 396.
[27] J. Shen, X. R. Qian, *Bioresources* **2012**, *7*, 4495.
[28] Z. Guo, W. Liu, B. L. Su, *J. Colloid Interf. Sci.* **2011**, *353*, 335.
[29] H. Ogihara, J. Xie, J. Okagaki, T. Saji, *Langmuir* **2012**, *28*, 4605.
[30] K. Abe, K. Suzuki, D. Citterio, *Anal. Chem.* **2008**, *80*, 6928.
[31] B. Balu, V. Breedveld, D. W. Hess, *Langmuir* **2008**, *24*, 4785.
[32] Q. He, C. Ma, X. Hu, H. Chen, *Anal. Chem.* **2012**, *85*, 1327.
[33] H. S. Khoo, F. G. Tseng, *Nanotechnology* **2008**, *19*, 345603.
[34] M. J. Oh, S. Y. Lee, K. H. Paik, *J. Ind. Eng. Chem.* **2011**, *17*, 149.
[35] A. Cunha, A. Gandini, *Cellulose* **2010**, *17*, 875.
[36] C. Gaiolas, A. P. Costa, M. Nunes, M. J. S. Silva, M. N. Belgacem, *Plasma Process. Polym.* **2008**, *5*, 444.
[37] G. R. J. Artus, S. Seeger, *Ind. Eng. Chem. Res.* **2012**, *51*, 2631.
[38] J. Zimmermann, F. A. Reifler, G. Fortunato, L.C. Gerhardt, S. Seeger, *Adv. Funct. Mater.* **2008**, *18*, 3662.
[39] M. A. Shirgholami, M. S. Khalil-Abad, R. Khajavi, M. E. Yazdanshenas, *J. Colloid Interf. Sci.* **2011**, *359*, 530.
[40] F. J. Norton, *Production of Water-Repellent Materials*, US Patent Office, 427/255.393, **1943**.
[41] D. Nystrom, J. Lindqvist, E. Ostmark, A. Hult, E. Malmstrom, *Chem. Commun.* **2006**, 3594.
[42] P. Jackson, *Folding Techniques for Designers. From Sheet to Form*, Laurence King Publishing Ltd, London, UK, **2011**.
[43] A. Tuteja, W. Choi, J. M. Mabry, G. H. McKinley, R. E. Cohen, *Proc. Natl. Acad. Sci. USA* **2008**, *105*, 18200.
[44] Z. G. Guo, W. M. Liu, B. L. Su, *J. Colloid Interf. Sci.* **2011**, *353*, 335.
[45] E. Wang, M. Bucaro, J. Taylor, P. Kolodner, J. Aizenberg, T. Krupenkin, *Microfluid. Nanofluid.* **2009**, *7*, 137.
[46] A. Sidorenko, T. Krupenkin, J. Aizenberg, *J. Mater. Chem.* **2008**, *18*, 3841.
[47] T. S. Wong, S. H. Kang, S. K. Y. Tang, E. J. Smythe, B. D. Hatton, A. Grinthal, J. Aizenberg, *Nature* **2011**, *477*, 443.
[48] G. A. Baum, D. R. Waterman, IPC Technical Paper Series, Institute of Paper Chemistry (Appleton, Wis.), Georgia Institute of Technology, **1986**, http://hdl.handle.net/1853/2693, accessed: June, 2013.
[49] P. Vernhes, M. Dube, J. F. Bloch, *Appl. Surf. Sci.* **2010**, *256*, 6923.
[50] P. Vernhes, J.-F. Bloch, A. Blayo, B. Pineaux, *J. Mater. Process. Technol.* **2009**, *209*, 5204.
[51] A. Voller, D. E. Bidwell, A. Bartlett, *Bull. World Health Organ.* **1976**, *53*, 55.
[52] C. D. Chin, T. Laksanasopin, Y. K. Cheung, D. Steinmiller, V. Linder, H. Parsa, J. Wang, H. Moore, R. Rouse, G. Umviligihozo, E. Karita, L. Mwambarangwe, S. L. Braunstein, J. van de Wijgert, R. Sahabo, J. E. Justman, W. El-Sadr, S. K. Sia, *Nat. Med.* **2011**, *17*, 1015.
[53] C. M. Cheng, A. W. Martinez, J. Gong, C. R. Mace, S. T. Phillips, E. Carrilho, K. A. Mirica, G. M. Whitesides, *Angew. Chem.* **2010**, *49*, 4771.
[54] E. Verpoorte, *Electrophoresis* **2002**, *23*, 677.
[55] E. M. Southern, *J. Mol. Biol.* **1975**, *98*, 503.
[56] M. A. Burns, B. N. Johnson, S. N. Brahmasandra, K. Handique, J. R. Webster, M. Krishnan, T. S. Sammarco, P. M. Man, D. Jones, D. Heldsinger, C. H. Mastrangelo, D. T. Burke, *Science* **1998**, *282*, 484.
[57] K. A. Mirica, S. T. Phillips, C. R. Mace, G. M. Whitesides, *J. Agric. Food Chem.* **2010**, *58*, 6565.
[58] R. S. Lanciotti, C. H. Calisher, D. J. Gubler, G. J. Chang, A. V. Vorndam, *J. Clin. Microbiol.* **1992**, *30*, 545.
[59] P. Yager, T. Edwards, E. Fu, K. Helton, K. Nelson, M. R. Tam, B. H. Weigl, *Nature* **2006**, *442*, 412.
[60] I. Meyvantsson, D. J. Beebe, *Annu. Rev. Anal. Chem.* **2008**, 1, 23.
[61] G. Kohler, C. Milstein, *Nature* **1975**, *256*, 495.
[62] J. Monod, *Annu. Rev. Microbiol.* **1949**, *3*, 371.
[63] Y. J. Sung, R. Farnood, *J. Ind. Eng. Chem.* **2007**, *13*, 225.
[64] A. W. Adamson, A. P. U. Gast, *Physical Chemistry of Surfaces*, Wiley, New York **1997**.
[65] G. R. J. Artus, S. Jung, J. Zimmermann, H.-P. Gautschi, K. Marquardt, S. Seeger, *Adv. Mater.* **2006**, *18*, 2758.
[66] P. G. De Gennes, F. Brochard-Wyart, D. Quere, *Capillarity and Wetting Phenomena: Drops, Bubbles, Pearls, Waves*, Springer, New York **2003**.
[67] G. L. E. Turner, *CRC Handbook of Chemistry and Physics*, 70th Ed., Vol. *48*, CRC Press, Boca Raton, FL **1991**.
[68] L. Feng, Y. Zhang, J. Xi, Y. Zhu, N. Wang, F. Xia, L. Jiang, *Langmuir* **2008**, *24*, 4114.
[69] M. J. Rosen, *Surfactants and Interfacial Phenomena*, John Wiley & Sons, Holboken **2004**.
[70] R. Lakes, *Adv. Mater.* **1993**, *5*, 293.
[71] A. K. Epstein, T. S. Wong, R. A. Belisle, E. M. Boggs, J. Aizenberg, *Proc. Natl. Acad. Sci. USA* **2012**, *109*, 13182.
[72] W. Ma, Y. Higaki, H. Otsuka, A. Takahara, *Chem. Commun.* **2013**, *49*, 597.
[73] A. C. Glavan, R. V. Martinez, E. J. Maxwell, A. B. Subramaniam, R. M. D. Nunes, S. Soh, G. M. Whitesides, *Lab Chip* **2013**,*13*, 2922.
[74] M. Rzechowicz, R. M. Pashley, *J. Colloid Interf. Sci.* **2006**, *298*, 321.
[75] P. Kim, T. S. Wong, J. Alvarenga, M. J. Kreder, W. E. Adorno-Martinez, J. Aizenberg, *ACS Nano* **2012**, *6*, 6569.